Photochemical synthesis of natural membrane lipids in artificial and living cells

Peng Ji[1], Alexander Harjung[1], Caroline Knittel[1], Alessandro Fracassi[1], Jiyue Chen[1], Neal K. Devaraj[1]*

[1]Department of Chemistry and Biochemistry, University of California, San Diego, 9500 Gilman Drive, La Jolla, California 92093, United States.

*Corresponding author. Email: ndevaraj@ucsd.edu

Abstract: A general method for the abiogenesis of natural lipids could transform the development of lifelike artificial cells and unlock new ways to explore lipid functions in living cells. However, it is unclear if mild non-enzymatic methods can be harnessed to synthesize the diverse array of lipids found in biology. Here, we demonstrate the abiotic formation of natural lipids in water using visible-light-driven photoredox chemistry. Radical-mediated coupling of hydrocarbon tails to polar single-chain precursors yields lipids identical to those enzymatically formed. Spatiotemporally controlled lipid generation promotes de novo vesicle formation, growth, and division. Several photoredox catalysts, including those activated by nucleic acids, can drive lipid synthesis. Additionally, we show that the synthesis of bioactive lipids can trigger signaling in living cells.

Main Text: Lipids are essential molecular components of all life on Earth. Membrane lipids define cellular boundaries, such as the plasma membrane, and were likely critical for early protocell compartmentalization (*1, 2*). Lipids play important roles in cell signaling, and their dysregulation often leads to disease (*3*). Cells synthesize lipids enzymatically, with a key step frequently being the acylation of a polar head group with a fatty hydrocarbon tail, catalyzed by a membrane protein (*4, 5*). Despite advances over the last decades, reconstituting biochemical lipid synthesis ex cellulo remains challenging (*6, 7*). A general strategy for synthesizing the wide range of membrane lipids found in biology under physiologically relevant conditions would have several applications in generating lipid-based materials. For instance, developing lifelike artificial cells will likely require integrating lipid compartment metabolism with nucleic acid replication and natural membrane lipids are intrinsically compatible with the necessary biological machinery. Additionally, the ability to produce specific biological lipids in cells would enable direct elucidation of lipid structure-function relationships in biology.

As an alternative to enzymatic synthesis, several studies have attempted to generate natural lipids, or very close analogs, abiotically in water (*8-14*). Previous approaches to abiotically generate natural lipids in water have used acylation chemistry to mimic the enzymatic synthesis of lipids (Fig. 1A-1B) (*12-14*). For instance, recent work has shown that lysophospholipids can be acylated in alkaline media to create natural lipids (Fig. 1A) (*14*). However, these methods have suffered from low yields, limited substrate scope, and the inability to generate membrane lipids under physiologically relevant conditions. In seeking a unified method to form a diverse array of natural lipids abiotically, we explored approaches distinct from the traditional acylation of polar head groups by activated fatty acids, as used both enzymatically and in previous synthetic methods. Since most lipids consist of hydrocarbon tails attached to a more polar functional group, a mechanism to directly ligate hydrocarbon tails to polar lipid precursors via carbon-carbon bond formation would be applicable for generating multiple natural lipids. Numerous studies have demonstrated that photoredox coupling chemistry is extremely attractive for achieving carbon-carbon bond formation due to its mild nature (*15*), the potential for spatiotemporal control (*16*), and studies that have demonstrated applicability to bioconjugation (*17, 18*), even in living cells (*19-21*). However, the feasibility of creating self-assembling lipid species in water through photoredox-mediated coupling remains uncertain.

Here we describe the photocatalytic synthesis of natural membrane lipids in water, leading to the spontaneous assembly of protocell vesicles. Photoredox lipid ligation (PLL) between *N*-hydroxyphtalimide (NHPI) fatty esters and olefin-modified lysolipids forms carbon-carbon bonds, generating natural lipids (Fig. 1C). Various organic photoredox catalysts, including those activated by nucleic acids, can trigger PLL. Light catalyzed synthesis of phospholipids in water leads to the de novo formation of protocells with biologically identical lipids in their membranes. Continuous irradiation of lipid precursors causes vesicle growth, budding, and division. Several lipid classes, including phospholipids, sphingolipids, and diacylglycerols, can be formed in water. In the presence of living cells, we demonstrate assembly of bioactive signaling lipids like ceramides and diacylglycerols. PLL shows promise for creating more lifelike artificial cell membranes and as a tool for understanding the roles of specific lipids in living cells.

Recent studies have demonstrated that the photoinduced oxidative decarboxylation of carboxylic acids can mediate radical carbon-carbon bond cross-coupling reactions in aqueous conditions. This method has been shown to have several promising applications in chemical biology, including DNA modification (*22*) and protein bioconjugation (*17*). Unfortunately, decarboxylative cross-coupling reactions often require air-free conditions, are sluggish, and, for the generation of lipids, would require the use of fatty acids as precursors, which are not bioorthogonal. Nevertheless, we initially explored adapting such reactions for natural lipid synthesis and unfortunately found that only trace quantities of the desired lipid products could be detected (table S1).

Rather than oxidative decarboxylation, we next turned to reductive decarboxylation. Since seminal work by Okada and coworkers (*23*), many groups have shown that photoredox driven

radical cross-coupling can take place by single electron transfer (SET) to NHPI esters derived from carboxylic acids (*24, 25*). Reductive fragmentation leads to the extrusion of carbon dioxide and generation of a carbon centered radical that can couple to a Michael-type acceptor (*26*). Recent studies have demonstrated that conjugation works in aqueous conditions and depending on the choice of photocatalyst, can be conducted with relatively benign visible light (>500 nm excitation), which is an important prerequisite for biocompatibility. To adapt reductive decarboxylative coupling for PLL, we synthesized an NHPI ester (**2a**) from myristic acid and the acrylate derivative of oleoyl-lysophosphatidyl choline (**1a**). We formed a thin film of these precursors, hydrated the film with PBS buffer, and added 5 mol% of eosin Y as a photocatalyst (Fig. 2A). As a reducing agent, we used three equivalents of 1-benzyl-1,4-dihydronicotinamide (BNAH), a well-known 1,4-dihydronicotinamide adenine dinucleotide (NADH) analog. No effort was made to exclude oxygen. When this mixture was irradiated by 525 nm LED light for 30 minutes, the natural phospholipid 1-oleoyl-2-palmitoyl-*sn*-glycero-3-phosphocholine (OPPC) (*27*) was readily detected by liquid chromatography mass spectrometry (LCMS), and an isolated product yield of 95% was obtained (Fig. 2B, entry 1).

We also explored alternative photocatalysts (Fig. 2B, table S3) and reducing agents (Fig. 2B, entry 1 and 4-8). Using rhodamine B as a photocatalyst did not significantly alter yields (92%, excitation 525 nm, Fig. 2B, entry 9). We observed OPPC formation with reduced yield (77%) under the irradiation of blue light (450 nm) in the absence of eosin Y (table S2), consistent with previous work showing that BNAH can act as its own photocatalyst (*15*). The choice of reducing agent was very important and switching BNAH with water soluble NADH (Fig. 2B, entry 6), ascorbate (Fig. 2B, entry 7), or *i*-Pr_2NEt (Figure 2B, entry 8) only yielded trace lipid products, which might be attributed to the colocalization of BNAH with the lipophilic precursors. Control experiments (Figure 2B, entry 2-3; Table S3, entry 7) confirmed that green light, photocatalyst, and reductant were all essential for PLL to take place. We also found that the reaction displays chemoselectivity despite the presence of NHPI esters, which have previously been used to activate carboxylic acids for coupling with amines (*28*). Running the reaction in DMEM cell media with 10% fetal bovine serum, which contains a high concentration of amino acids (~6 mM), among other reagents needed for cell growth, did not compromise reaction efficiency significantly (Fig. 2B, entry 10). In mixtures of **1a**, **2a**, and BNAH, we observed good stability of the NHPI ester over 10 minutes when incubated with 1 mM lysine, 0.5 mM sphingosine, or DMEM buffer (fig. S3). We hypothesize that the selectivity and high yield of reaction can be attributed to the self-assembling nature of the long-chain lipophilic reagents, which likely form structures such as micelles or emulsion droplets in which the reactive groups are positioned in close local proximity to one another and exclude highly polar reagents like amino acids. In contrast, if non-amphiphilic olefins are reacted, such as *N*-acryloylglycine, photodriven ligation with NHPI ester **2a** did not take place (scheme S2). The rapid kinetics of PLL (Fig. 3C and fig. S4) also likely contributes to the observed selectivity.

There are multiple lipid classes in cells such as phospholipids, sphingolipids, and diacylglycerols (*29*). The mechanism of PLL suggests flexibility in the type of lipids that can be generated, provided that the target natural lipid possesses a fatty acyl tail. Changing the NHPI ester and the lipid olefin precursors enabled the synthesis of numerous phosphatidylcholines with either saturated (**3e** in Fig. 2C and **3k** in scheme S1), unsaturated (**3a** in Fig. 2A; **3b**, **3c** in Fig. 2C; **3j** in scheme S1) or polyunsaturated hydrocarbon tails (**3d** in Fig. 2C). We were able to show that alternative lipid head groups could also be used. For instance, PLL yielded diacylglycerol (**3i** in Fig. 2C) and phosphatidic acid (**3f** in Fig. 2C) in aqueous conditions, albeit in lower yields compared to phosphatidylcholines. Sphingolipids are a class of lipids highly enriched in the nervous system and are involved in several biological processes and diseases (*30*). Sphingolipids have an *N*-acyl fatty tail as opposed to phospholipids which typically possess hydrocarbon tails appended through *O*-acylation. To generate sphingolipids, we synthesized the acrylamide-containing lipid precursors **1e** and **1f**. Using a similar PLL approach, we were able to assemble sphingomyelin (**3g** in Fig. 2C), a major constituent of myelin sheaths, and ceramide (**3h** in Fig. 2C), a signaling sphingolipid involved in apoptosis (*31*).

As lipid synthesis takes place in water, we suspected that PLL would lead to de novo protocell vesicle formation (Fig. 3A). Since lysophospholipids can act as vesicle disrupting agents, to generate vesicles using PLL we used a slight excess of the NHPI ester. A mixture consisting of **1b** (0.83 mM), **2b** (1.25 mM), BNAH (2.5 mM), and eosin Y (0.05 mM) was irradiated in PBS. As expected, neither **1b** or **2b** on their own or combined formed giant vesicles (fig. S5), as determined by phase contrast light microscopy. Mixing all components of the reaction on a glass slide does not lead to observable vesicles if allowed to stand for 1 hour in the absence of light (Fig. 3D middle). However, if the same mixture is exposed to green LED light for 1 hour on a glass slide, large vesicles are readily observed under phase contrast microscopy (Fig. 3D, fig. S6), in agreement with our LCMS data indicating that 1-palmitoyl-2-oleoyl-*sn*-glycero-3-phosphocholine (POPC) lipid synthesis takes place in high yield (Fig. 3B). Interestingly, we also found that the photocatalyst eosin Y, itself fluorescent, is spontaneously encapsulated within vesicles during de novo vesicle formation (Fig. 3E, fig. S8-S9). We next characterized the de novo formed lipid vesicles generated by PLL. As a representative example, we chose to form OPPC vesicles through PLL as OPPC is a well-studied natural lipid that has been used extensively to make lipid vesicles (*32*). CryoEM of OPPC vesicles resulting from PLL revealed membrane bound spherical structures, with a membrane thickness (4.59 ± 0.07 nm) comparable to previous measurements (Fig. 3F, fig. S10-S11) (*33*). Additionally, PLL could take place in the presence of fluorescent proteins such as mCherry (Fig. 3G), and some of the proteins were spontaneously encapsulated within the vesicles formed. Similar to POPC vesicles, OPPC vesicles formed by PLL encapsulate the eosin Y photocatalyst spontaneously during reaction (Fig. 3H). De novo formed vesicles of OPPC containing eosin Y remain catalytically active and could generate new lipids by PLL. We removed unbound eosin Y and exposed vesicles containing spontaneously internalized eosin Y to all the PLL reactants except the eosin Y photocatalyst. Alternative lysolipid and NHPI precursors (**1a** and **2b**) were selected to afford a lipid product that could be easily distinguished from OPPC.

After irradiation with green LED light, 1,2-dioleoyl-*sn*-glycero-3-phosphocholine, **3c** (DOPC) synthesis was detected with 20% yield after 10 min (fig. S12-S13). Thus, de novo formed protocells are themselves catalytic for additional lipid synthesis (fig. S14).

The light-driven nature of PLL offers the potential for spatiotemporal control over lipid synthesis. Microscope focused excitation of eosin Y (bandpass filter 530-580 nm) in a solution of NHPI ester **2b** and lysolipid **1b** on a glass slide to form POPC led to localized de novo vesicle formation (Fig. 3D, fig. S6, movie S1). Several morphological transformations were observed upon continued illumination, including vesicle tubulation, budding, and division (Fig. 3I; fig. S7; movie S1, S4, and S5). These changes are likely due to additional lipid synthesis within the illumination region. Lipid precursors would be expected to continuously diffuse from the non-illuminated to the illuminated region. As new lipids are formed, expansion of preexisting membranes occurs. Controls without light or eosin Y photocatalyst did not yield de novo vesicle formation (movie S2 and S3). Living cell membranes contain a large diversity of lipid species. We found that PLL allows de novo formation of membranes containing multiple lipid species from a mixture of saturated and unsaturated NHPI precursors. Mixing an equivalent amount of two different NHPI esters (**2a** and **2b**) with four equivalents of lysolipid (**1b**), followed by green light irradiation, resulted in the formation of vesicles composed of both DPPC and POPC (1:1.7) (fig. S15-S17).

It has been suggested that linking nucleic acid replication to lipid vesicle growth and division would offer a possible pathway for generating protocells capable of Darwinian evolution (*1*). Thus, a longstanding goal in artificial cell research has been the discovery of mechanisms by which nucleic acids can be linked to protocell vesicle formation (*34, 35*). While previous studies have shown that the presence of DNA or RNA can affect lipid structures, we are not aware of mechanisms by which nucleic acids can catalyze the synthesis of lipids and subsequent protocell assembly. Since organic dyes such as eosin Y and rhodamine B can be used for PLL, we hypothesized that dyes that become activated in the presence of nucleic acids, such as intercalating dyes and aptamer binding fluorogens, might catalyze natural lipid synthesis by PLL in a manner that is dependent on the presence of specific nucleic acids. To test this hypothesis, we screened several DNA/RNA binding dyes for the ability to trigger PLL. A well-known class of activatable nucleic acid binding dyes are thiazole orange (TO) and its many related derivatives (*36*). These dyes bind to nucleic acids, typically by intercalating between bases. Binding restricts conformational changes, preventing very rapid non-radiative decay and leading to activation (*37*). We found that the DNA binding dyes TOTO-1 (thiazole orange homodimer), when intercalated into DNA, could act as a photocatalyst for the synthesis of POPC and trigger de novo vesicle formation (Fig. 4B-4C, fig. S18-S19). In the absence of DNA, no POPC synthesis was observed (Fig 4B). TO derivatives have also been shown to be activated by RNA aptamers. Unlike DNA intercalators, binding is highly dependent on the specific sequence and structure of the RNA (*38*). For instance, TO1-3PEG Desthiobiotin (TO1-Dbt) binds to and is activated by the evolved RNA aptamer Mango-II in a sequence dependent manner (*39, 40*). Similar to our results with DNA, we

found that lipid synthesis and de novo vesicle formation could be catalyzed by PLL in the presence of the Mango-II aptamer and TO1-Dbt dye (Figure 4A-4C, fig. S18 and S20). No lipid synthesis could be detected in the presence of either aptamer or dye alone (Fig 4B). Our findings suggest the PLL provides a novel mechanism by which lipid metabolism and nucleic acid replication may be linked, and we are currently determining the extent to which PLL can be driven by alternative dye activating nucleic acids.

Mammalian cells enzymatically generate thousands of unique lipids (*41*). A major challenge has been deciphering not just the identity of specific lipids but determining how specific changes in chemical structure affect their biological function. Dysregulation of lipid metabolism often leads to the accumulation of specific toxic lipids and disease, but the molecular mechanisms of lipid toxicity are often obscure (*42*). The ability to generate specific lipids in living cells would provide a tool for improving our understanding of lipid structure-function relationships. Based on the observed selectivity of PLL, and previous studies showing cell compatibility for photocatalysis using eosin Y (*43*), we speculated that PLL might be capable of synthesizing specific lipids in the presence of living cells. To initially determine live cell compatibility, we designed a simple experiment by which cells (HeLa) were exposed to synthetic NHPI lipid ester **2e** bearing a terminal azide group along with acrylate modified lysophosphatidylcholine **1b**. Cells were also exposed to eosin Y photocatalyst and the reducing agent. If synthesis of azido-phospholipid **3m** (fig. S22) takes place by PLL, the product phospholipid would be expected to be more easily retained in cell membranes compared to the single-chain precursors. After a washing step, the presence of azido-phospholipids in the membrane was monitored by labeling of the azide groups with a fluorescent cyclooctyne dye (Fig. 5A). Cells were treated with lipid precursors, irradiated with 525 nm LED light for 5 minutes, and washed with cell media. Subsequent staining with cyclooctyne DBCO-Fluor 594 revealed significant membrane modification (Fig. 5B). In the absence of light or lysolipid **1b**, significantly less staining was observed (Fig. 5B and fig. S22), likely due to the ability of the single-chain precursors to be washed out more readily than the phospholipid product.

Having determined cell compatibility, we next sought to determine if PLL could generate bioactive lipids in living cell membranes. We initially tested the synthesis of ceramide, which is a central molecule in sphingolipid biosynthesis and has been shown to play a key role in apoptosis (*44, 45*). While ceramides and synthetic analogs have been extensively studied, the poor solubility of native *N*-acyl ceramides renders them unable to cross the cell membrane and has impeded studies on how the chemical structure of ceramides affects their cellular function. We designed a deuterated NHPI ester **2d** that can be coupled to acrylamide modified sphingosine **1f** via PLL to generate an isotopically labeled ceramide species **3n**. Deuterated ceramide can be differentiated from native ceramide by quantitative high-resolution mass spectrometry. We performed PLL to synthesize deuterated ceramides in HeLa cells, followed by a total lipid extraction and analysis of product formation by mass spectrometry, which revealed the formation of physiological quantities of ceramide (Fig. 5C and fig. S23-S24). Furthermore, photogeneration of ceramide led to a reduction in cell viability compared to several controls and in agreement with previously reported

results (Fig. 5D). Past work has shown that sphingosine itself can trigger apoptosis. However, we found that the acrylamide-modified sphingosine **1f** showed reduced toxicity (Fig. S25), highlighting an advantage of using abiotic precursors. The external addition of ceramide did not reduce cell viability (Fig. 5D), as expected given its poor membrane permeability. The lack of activity from externally added ceramide also suggests that the photochemical synthesis of ceramide species takes place within cells, aided by the improved cellular permeability of the single-chain precursors.

As previously discussed, PLL can also be used to synthesize natural diacylglycerols (DAGs), which comprise an important class of lipid signaling molecules. DAGs activate enzymes in the protein kinase C (PKC) family, leading to phosphorylation of a wide range of downstream protein targets. Recent work has suggested that the location, timing, and structure of diacylglycerols significantly affect downstream signaling events and their impact on cell function (*46*). We performed PLL to form 1-2-dioleoyl-sn-glycerol **3i** in the presence of HeLa cells and monitored the phosphorylation of protein targets of PKC adapting a previously developed western-blot assay (*47*). Light-mediated formation of diacylglycerol **3i** led to significant upregulation of target protein phosphorylation (Fig. 5E and fig. S26), nearly close to that obtained using PKC activator phorbol 12,13-dibutyrate (PDBu) as a positive control (fig. S26). PKC inhibition using 1 μM Gö 6983, a pan PKC inhibitor, dramatically decreased the observed phosphorylation (Fig. 5E) (*48*). Running the reaction protocol while avoiding light significantly decreased phosphorylation (Fig. 5E). However, we did observe slight PKC activation above background, likely due to the acrylate monoacylglycerol precursor **1g** (fig. S26) and any inadvertent exposure to light during cell handling. Overall, our results suggest that PLL can be used to generate a variety of lipids in living systems and creates several opportunities for studying specific lipid species and their effect on cellular function.

References and Notes:

1. J. W. Szostak, D. P. Bartel, P. L. Luisi, Synthesizing life. *Nature* **409**, 387-390 (2001).
2. G. F. Joyce, J. W. Szostak, Protocells and RNA self-replication. *Cold Spring Harb. Perspect. Biol.* **10**, a034801 (2018).
3. M. P. Wymann, R. Schneiter, Lipid signalling in disease. *Nat. Rev. Mol. Cell Biol.* **9**, 162-176 (2008).
4. J. C. M. Holthuis, A. K. Menon, Lipid landscapes and pipelines in membrane homeostasis. *Nature* **510**, 48-57 (2014).
5. T. Harayama, H. Riezman, Understanding the diversity of membrane lipid composition. *Nat. Rev. Mol. Cell Biol.* **19**, 281-296 (2018).
6. M. Exterkate, A. Caforio, M. C. A. Stuart, A. J. M. Driessen, Growing membranes in vitro by continuous phospholipid biosynthesis from free fatty acids. *ACS Synth. Biol.* **7**, 153-165 (2018).
7. D. Blanken, D. Foschepoth, A. C. Serrão, C. Danelon, Genetically controlled membrane synthesis in liposomes. *Nat. Commun.* **11**, 4317 (2020).

8. I. Budin, N. K. Devaraj, Membrane assembly driven by a biomimetic coupling reaction. *J. Am. Chem. Soc.* **134**, 751-753 (2012).
9. R. J. Brea, C. M. Cole, N. K. Devaraj, In situ vesicle formation by native chemical ligation. *Angew. Chem. Int. Ed.* **53**, 14102-14105 (2014).
10. J. Flores *et al.*, Rapid and sequential dual oxime ligation enables de novo formation of functional synthetic membranes from water-soluble precursors. *Angew. Chem. Int. Ed.* **61**, e202200549 (2022).
11. J. Chen *et al.*, Rapid formation of non-canonical phospholipid membranes by chemoselective amide-forming ligations with hydroxylamines. *Angew. Chem. Int. Ed.* **63**, e202311635 (2024).
12. A. Bhattacharya *et al.*, Chemoselective esterification of natural and prebiotic 1,2-amino alcohol amphiphiles in water. *J. Am. Chem. Soc.* **145**, 27149-27159 (2023).
13. A. K. Rudd, N. K. Devaraj, Traceless synthesis of ceramides in living cells reveals saturation-dependent apoptotic effects. *Proc. Natl. Acad. Sci. U.S.A.* **115**, 7485-7490 (2018).
14. L. Liu *et al.*, Enzyme-free synthesis of natural phospholipids in water. *Nat. Chem.* **12**, 1029-1034 (2020).
15. R. Chowdhury *et al.*, Decarboxylative alkyl coupling promoted by NADH and blue light. *J Am. Chem. Soc.* **142**, 20143-20151 (2020).
16. S. Aubert, M. Bezagu, A. C. Spivey, S. Arseniyadis, Spatial and temporal control of chemical processes. *Nat. Rev. Chem.* **3**, 706-722 (2019).
17. S. Bloom *et al.*, Decarboxylative alkylation for site-selective bioconjugation of native proteins via oxidation potentials. *Nat. Chem.* **10**, 205-211 (2018).
18. B. Josephson *et al.*, Light-driven post-translational installation of reactive protein side chains. *Nature* **585**, 530-537 (2020).
19. J. B. Geri *et al.*, Microenvironment mapping via Dexter energy transfer on immune cells. *Science* **367**, 1091-1097 (2020).
20. A. D. Trowbridge *et al.*, Small molecule photocatalysis enables drug target identification via energy transfer. *Proc. Natl. Acad. Sci. U.S.A.* **119**, e2208077119 (2022).
21. J. Niu *et al.*, Engineering live cell surfaces with functional polymers via cytocompatible controlled radical polymerization. *Nat. Chem.* **9**, 537-545 (2017).
22. D. K. Kölmel, R. P. Loach, T. Knauber, M. E. Flanagan, Employing photoredox catalysis for DNA-Encoded chemistry: decarboxylative alkylation of α-amino acids. *ChemMedChem* **13**, 2159-2165 (2018).
23. K. Okada, K. Okamoto, N. Morita, K. Okubo, M. Oda, Photosensitized decarboxylative Michael addition through N-(acyloxy)phthalimides via an electron-transfer mechanism. *J. Am. Chem. Soc.* **113**, 9401-9402 (1991).
24. J. Schwarz, B. König, Metal-free, visible-light-mediated, decarboxylative alkylation of biomass-derived compounds. *Green Chem.* **18**, 4743-4749 (2016).
25. S. Murarka, N-(Acyloxy)phthalimides as redox-active esters in cross-coupling reactions. *Adv. Synth. Catal.* **360**, 1735-1753 (2018).
26. S. K. Parida *et al.*, Single electron transfer-induced redox processes involving n-(acyloxy)phthalimides. *ACS. Catal.* **11**, 1640-1683 (2021).
27. H. Kuge, K. Akahori, K.-i. Yagyu, K. Honke, Functional compartmentalization of the plasma membrane of neurons by a unique acyl chain composition of phospholipids. *J. Biol. Chem.* **289**, 26783-26793 (2014).

28. G. H. L. Nefkens, G. I. Tesser, a novel activated ester in peptide syntheses. *J. Am. Chem. Soc.* **83**, 1263-1263 (1961).
29. B. Brügger, Lipidomics: analysis of the lipid composition of cells and subcellular organelles by electrospray ionization mass spectrometry. *Annu. Rev. Biochem.* **83**, 79-98 (2014).
30. Y. A. Hannun, L. M. Obeid, Sphingolipids and their metabolism in physiology and disease. *Nat. Rev. Mol. Cell Biol.* **19**, 175-191 (2018).
31. M. Verheij *et al.*, Requirement for ceramide-initiated SAPK/JNK signalling in stress-induced apoptosis. *Nature* **380**, 75-79 (1996).
32. A. M. Hanel, S. Schuettel, M. H. Gelb, Processive interfacial catalysis by mammalian 85-kilodalton phospholipase A2 enzymes on product-containing vesicles: Application to the determination of substrate preferences. *Biochemistry* **32**, 5949-5958 (1993).
33. E. Rideau, R. Dimova, P. Schwille, F. R. Wurm, K. Landfester, Liposomes and polymersomes: a comparative review towards cell mimicking. *Chem. Soc. Rev.* **47**, 8572-8610 (2018).
34. K. Kurihara *et al.*, A recursive vesicle-based model protocell with a primitive model cell cycle. *Nat. Commun.* **6**, 8352 (2015).
35. K. Kurihara *et al.*, Self-reproduction of supramolecular giant vesicles combined with the amplification of encapsulated DNA. *Nat. Chem.* **3**, 775-781 (2011).
36. J. Nygren, N. Svanvik, M. Kubista, The interactions between the fluorescent dye thiazole orange and DNA. *Biopolymers* **46**, 39-51 (1998).
37. G. L. Silva, V. Ediz, D. Yaron, B. A. Armitage, Experimental and computational investigation of unsymmetrical cyanine dyes: understanding torsionally responsive fluorogenic dyes. *J. Am. Chem. Soc.* **129**, 5710-5718 (2007).
38. E. V. Dolgosheina *et al.*, RNA Mango aptamer-fluorophore: a bright, high-affinity complex for RNA labeling and tracking. *ACS Chem. Biol.* **9**, 2412-2420 (2014).
39. A. Autour *et al.*, Fluorogenic rna mango aptamers for imaging small non-coding rnas in mammalian cells. *Nat. Commun.* **9**, 656 (2018).
40. S. S. S. Panchapakesan, S. C. Y. Jeng, P. J. Unrau, Purification of rna mango tagged native rna-protein complexes from cellular extracts using to1-desthiobiotin fluorophore ligand. *Bio. Protoc.* **8**, e2799 (2018).
41. O. Quehenberger *et al.*, Lipidomics reveals a remarkable diversity of lipids in human plasma 1 [S]. *J. Lipid Res.* **51**, 3299-3305 (2010).
42. S. Spassieva, E. Bieberich, Lysosphingolipids and sphingolipidoses: Psychosine in Krabbe's disease. *J. Neurosci. Res.* **94**, 974-981 (2016).
43. Y. Li, M. B. Aggarwal, K. Nguyen, K. Ke, R. C. Spitale, Assaying RNA localization in situ with spatially restricted nucleobase oxidation. *ACS Chem. Biol.* **12**, 2709-2714 (2017).
44. S. Dadsena *et al.*, Ceramides bind VDAC2 to trigger mitochondrial apoptosis. *Nat. Commun.* **10**, 1832 (2019).
45. S. A. F. Morad, M. C. Cabot, Ceramide-orchestrated signalling in cancer cells. *Nat. Rev. Cancer* **13**, 51-65 (2013).
46. K. Kolczynska, A. Loza-Valdes, I. Hawro, G. Sumara, Diacylglycerol-evoked activation of PKC and PKD isoforms in regulation of glucose and lipid metabolism: a review. *Lipids Health Dis.* **19**, 113 (2020).
47. G. Lordén *et al.*, Enhanced activity of Alzheimer disease-associated variant of protein kinase Cα drives cognitive decline in a mouse model. *Nat. Commun.* **13**, 7200 (2022).

48. M. Gschwendt *et al.*, Inhibition of protein kinase C μ by various inhibitors. Inhibition from protein kinase c isoenzymes. *FEBS Lett.* **392**, 77-80 (1996).
49. R. J. Trachman, III *et al.*, Crystal structures of the Mango-II RNA aptamer reveal heterogeneous fluorophore binding and guide engineering of variants with improved selectivity and brightness. *Biochemistry* **57**, 3544-3548 (2018).

Acknowledgments: The authors acknowledge the facilities along with the scientific and technical assistance of the staff of the cryoEM facility at UCSD. The UCSD molecular mass spectrometry facility is acknowledged. We also acknowledge helpful discussions with Prof. Itay Budin and Prof. Nate Romero. **Funding**: This work was funded by the Department of Defense (N00014-22-1-2800 ONR VBFF), the National Institutes of Health (R35GM141939) and the Alfred P. Sloan Foundation (2022-19397). **Author contributions**: Conceptualization: P.J. and N.K.D. Methodology: P.J. Investigation: P.J., A.H., C.K., J.C.. Visualization: P.J. Funding acquisition: N.K.D. Supervision: N.K.D. Writing – original draft: P.J. and N.K.D. Writing – review & editing: P.J., A.F., A.H., N.K.D. **Competing interests**: The authors declare that they have no competing interests.

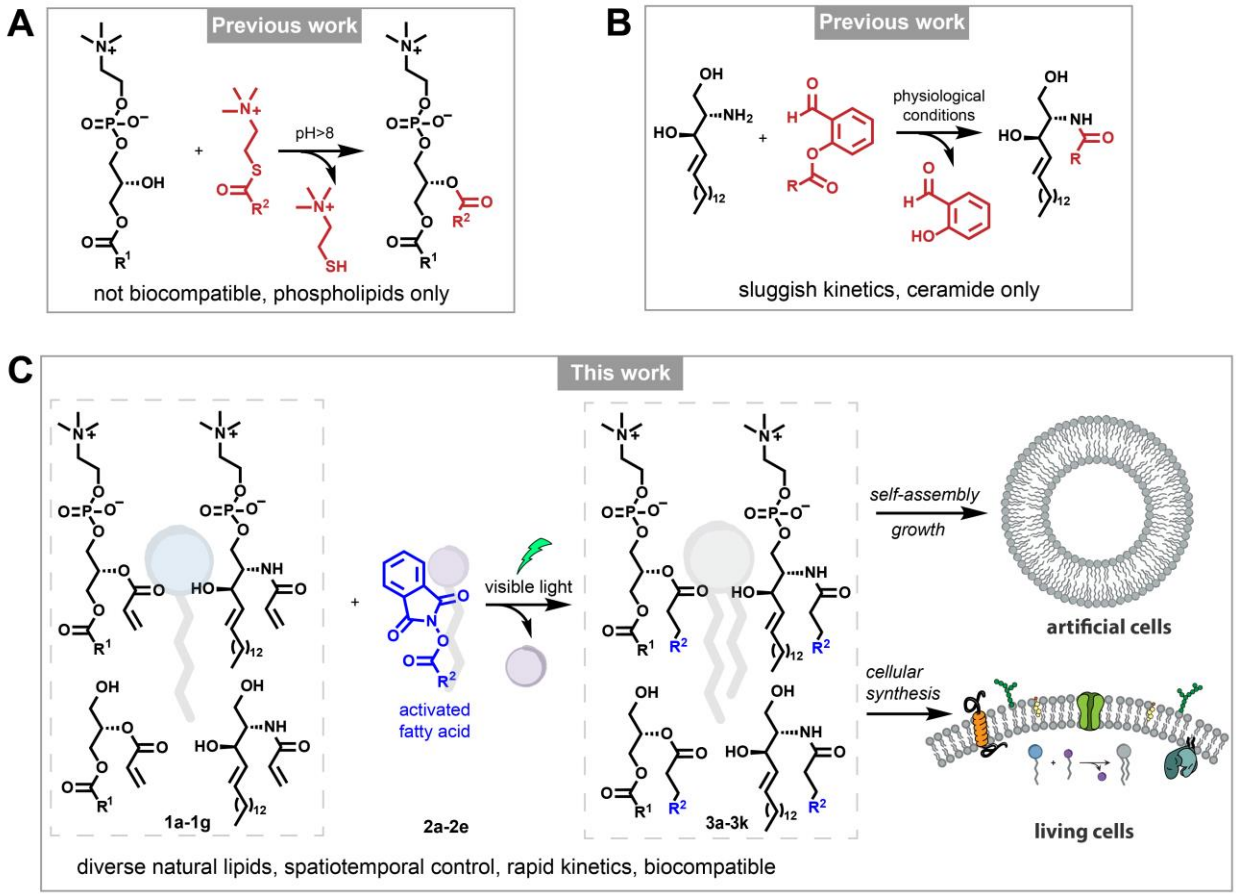

Fig. 1. Abiotic synthesis of natural membrane lipids in water. (A) Enzyme-free synthesis of natural phospholipids under prebiotically relevant alkaline conditions. (B) Traceless synthesis of ceramide by acylation of sphingosine in living cells. (C) Unified strategy for the synthesis of a wide range of natural lipids in artificial and living cells through photoredox lipid ligation (PLL) (this work).

B

Entry	Deviation from standard conditions[a]	Yield (%)[b]
1	None	95[c]
2	No light	trace
3	No eosin Y	trace
4	Decyl-NAH instead of BNAH	97
5	BuNAH instead of BNAH	80
6	NADH instead of BNAH	trace
7	Ascorbate instead of BNAH	trace
8	DIPEA instead of BNAH	trace
9	RhodB instead of eosin Y	92
10	DMEM (no phenol red) instead of PBS	94

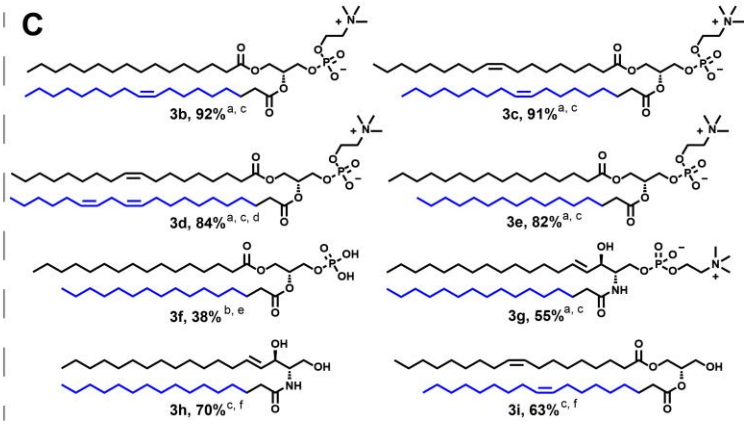

Fig. 2. Reaction condition optimization and selected scope of natural lipids synthesized by PLL. (A) Reaction in PBS buffer between 18:1-lyso-PC-acrylate **1a** and NHPI ester **2a** under green light, generating natural phospholipid OPPC **3a**. The protocol shown represents the standard conditions. (B) Reaction condition optimization using different reductants and photocatalysts as well as controls. (C) Representative examples of natural lipids (phosphatidylcholines, sphingolipids, diacylglycerol) formed by PLL. Additional chemical structures can be found in table S2. [a]Reaction conditions unless specified: a mixture of lysolipid **1** (2 mM), NHPI ester **2** (1 mM), BNAH (3 mM), and eosin Y (5 mol%) in PBS was irradiated by green light (525 nm) for 30 min at room temperature. [b]HPLC yield. [c]Isolated yield. [d]Reaction time is 15 min. [e]The reaction was performed without eosin Y under blue light (450 nm). [f]**1g** or **1f** (1 mM), NHPI ester **2** (2 mM), BNAH (3 mM), 1-oleoyl-2-hydroxy-*sn*-glycero-3-phosphocholine (18:1-lyso-PC) (3 mM), eosin Y (0.05 mM) in H_2O under green light for 30 min at room temperature.

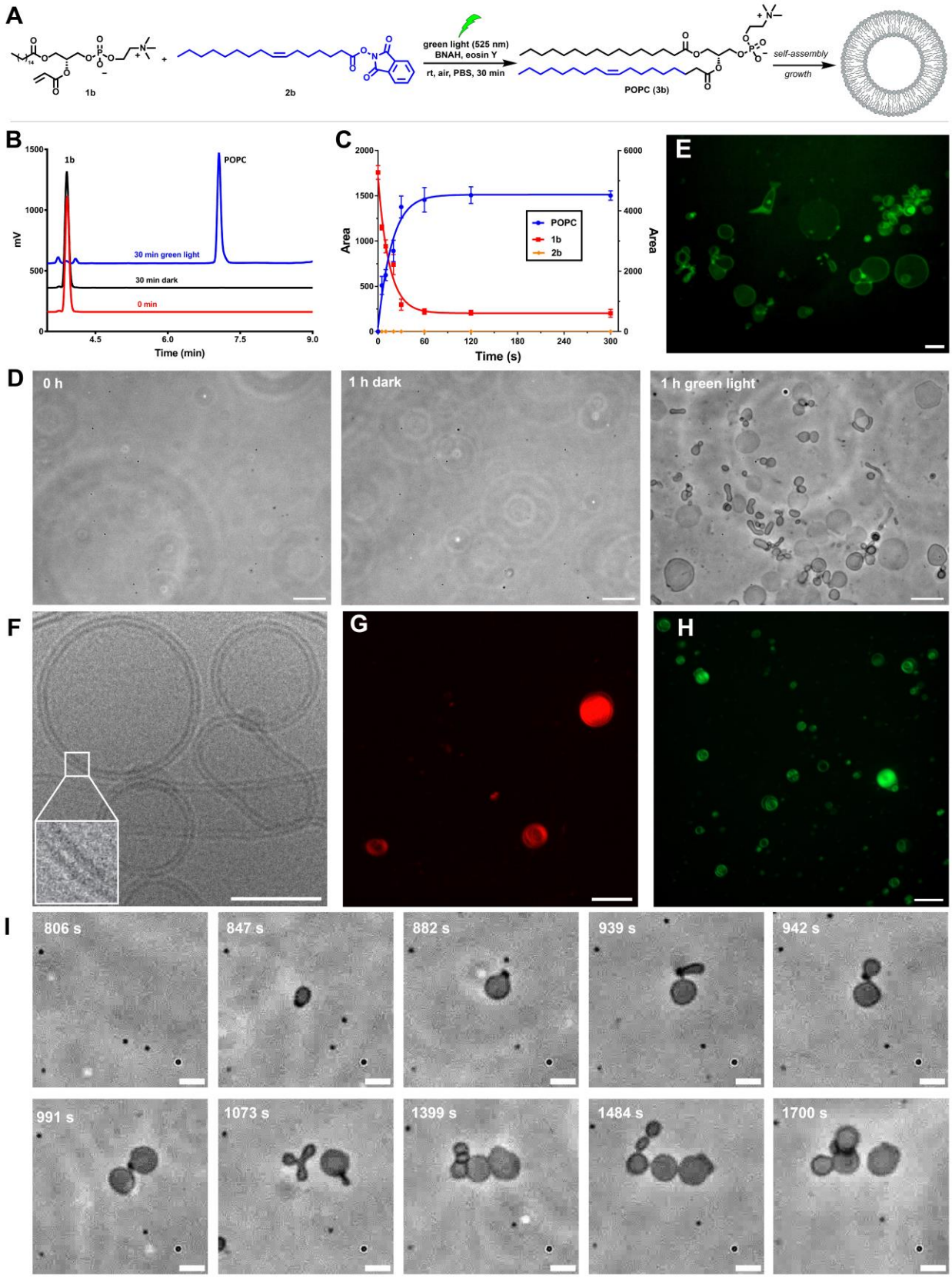

Fig. 3. De novo formation of protocell vesicles in water by PLL. (A) Scheme depicting light-triggered reaction between lysolipid **1b** and NHPI ester **2b** forming POPC **3b** which self-assembles to form lipid vesicles. (B) ELSD-HPLC traces of POPC synthesis under green light. The reaction consisted of **1b** (2 mM), **2b** (1 mM), BNAH (3 mM), eosin Y (0.05 mM) in PBS for 30 min (blue line). In the absence of irradiation, no product was detected (black line). (C) Kinetics studies of POPC synthesis in PBS. The area of the ELSD signal for **1b**, **2b**, and POPC was calculated at the indicated time points. Left y axis is the area of the ELSD signal of **2b** and POPC. Right y axis is the area of the ELSD signal of **1b**. Error bars represent standard deviation (n = 3). (D) Phase contrast microscopy images of localized de novo POPC vesicle formation on a glass slide before and after irradiation with green light for 1 hour. Control in the absence of irradiation is also shown. The reaction mixture consisted of **1b** (0.83 mM), **2b** (1.25 mM), BNAH (2.5 mM), and eosin Y (0.05 mM) in PBS. Scale bar, 20 μm. (E) Confocal microscopy image showing eosin Y localization during de novo POPC vesicle formation on the glass slide. Eosin Y appears to be localized on or within protocell vesicle membranes. Scale bar, 10 μm. (F) A representative cryo-EM image of vesicles formed during the synthesis of OPPC **3a** by PLL confirming the presence of a phospholipid bilayer structure. Scale bar, 25 nm. (G) Fluorescence microscopy images demonstrating that in situ generation of OPPC vesicles in the presence of fluorescent protein mCherry leads to spontaneous protein encapsulation. The unencapsulated protein was removed by Ni-NTA beads before vesicles were imaged by confocal microscopy. Scale bar, 20 μm. (H) Fluorescence microscopy images demonstrating that in situ generation of OPPC vesicles leads to spontaneous retention of the eosin Y photocatalyst. The vesicles were imaged directly after PLL without attempting to remove unbound dye. Scale bar 20 μm. (I) Time-lapse phase contrast microscopy images during de novo POPC protocell vesicle formation under localized green light excitation (530-580 nm). Vesicle growth, budding, and division events can be observed during irradiation. Scale bar, 5 μm.

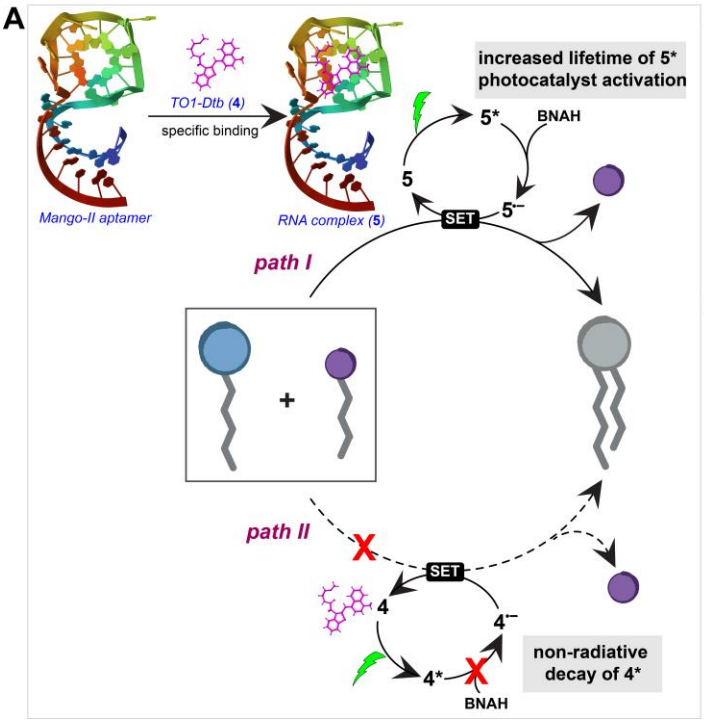

B

Nucleic acid	Conditions	POPC Yield (%)
DNA	DNA (30 ng/μL) + TOTO-1 (15 μM) + light	54 ± 13
	DNA (30 ng/μL) + TOTO-1 (15 μM) no light	0
	DNA (30 ng/μL) only + light	0
	TOTO-1 (15 μM) only + light	0
RNA	Mango-II (30 ng/μL) + TO1-Dtb (15 μM) + light	39 ± 5
	Mango-II (30 ng/μL) + TO1-Dtb (15 μM) no light	0
	Mango-II (30 ng/μL) only + light	0
	TO1-Dtb (15 μM) only + light	0

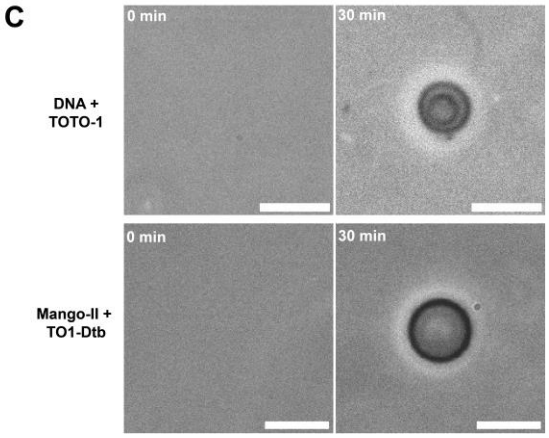

Fig. 4. Nucleic acid directed natural phospholipid synthesis under green light irradiation. (A) Mango-II aptamer binds and activates TO1-Dtb, which can act as a photoredox catalyst for PLL. In the absence of the RNA aptamer, TO1-Dtb is deactivated and unable to effectively catalyze lipid synthesis. Schematic illustration of aptamer and binding ligand adapted from PDB ID: 6C63 (*49*). (B) Nucleic acids (DNA and RNA aptamer) when bound to thiazole orange dyes catalyze the synthesis of POPC from **1b** (2 mM), **2b** (1 mM), BNAH (3 mM), under green light in PBS buffer. (C) Phase contrast microscopy images of representative lipid vesicles formed by nucleic acid/dye triggered PLL. Scale bar, 10 μm.

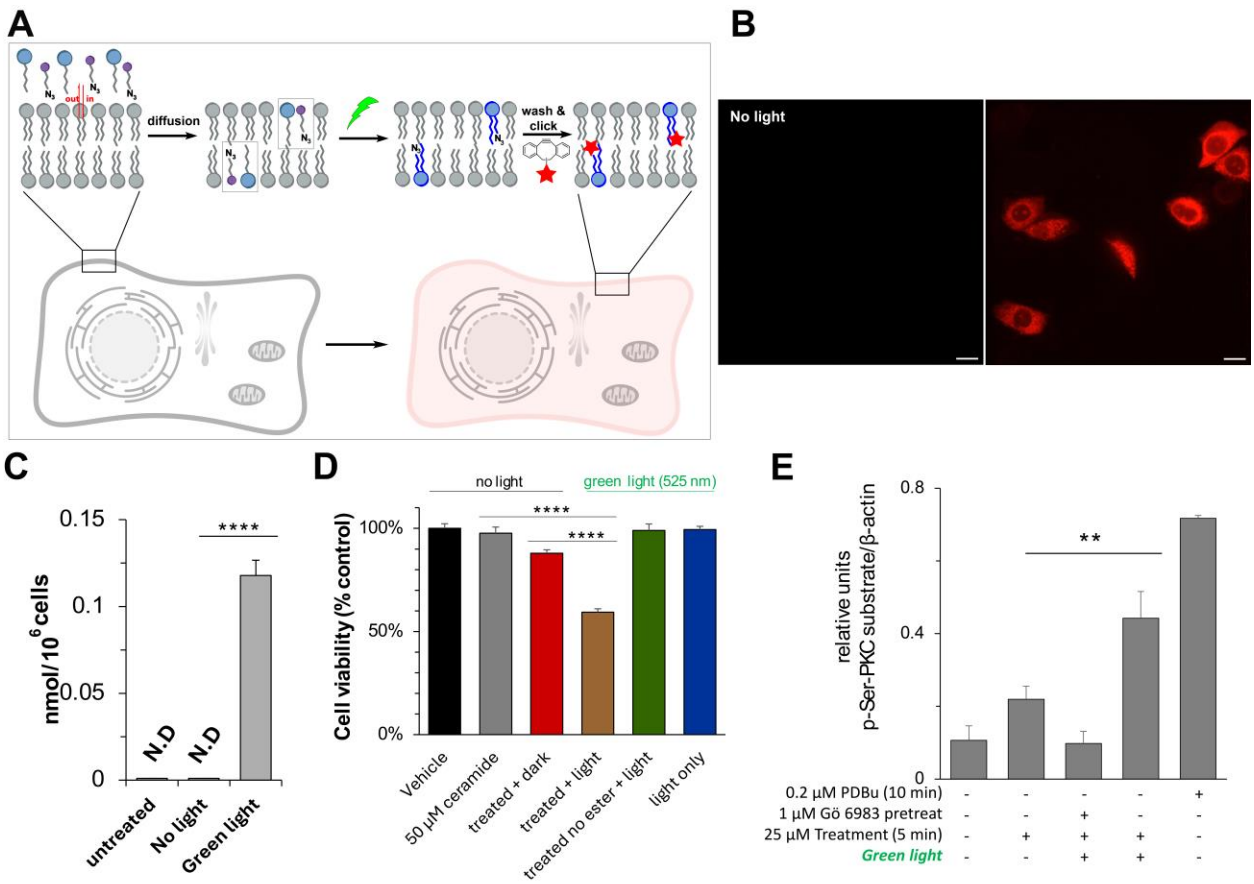

Fig. 5. Application of PLL in the presence of living cells. (A) Schematic illustration of PLL in cells. (B) Confocal images of HeLa cells after treatment with **1b**, azido-NHPI ester **2e**, BNAH, and eosin Y for 5 minutes followed by irradiation with 525 nm LED light for 30 minutes. After washing, HeLa cells were treated with DBCO-Fluor 594, washed, and then imaged by confocal microscopy. Scale bar, 20 µm. (C) Quantitative HRMS analysis of ceramide-d_{27} synthesis in cells by PLL. HeLa cells were treated with 100 µM **1f**, 200 µM **2d**, 300 µM BNAH, and 5 µM eosin Y in DMEM followed by irradiation with green light for 5 min. (D) Cell proliferation assay (CCK-8) of HeLa cells after light-controlled synthesis of ceramide. HeLa cells were treated with 50 µM **1f**, 100 µM **2a**, 150 µM BNAH, and 2.5 µM eosin Y in DMEM followed by irradiation with green light for 5 min. (E) Western blot assay analyzing the relative amount of phosphorylated-Ser PKC substrates between 63-75 kDa. PLL synthesis of 1-2-dioleoyl-*sn*-glycerol leads to the selective activation of the PKC pathway in HeLa cells. HeLa cells treated with 25 µM **1g**, 50 µM **2b**, 75 µM BNAH, and 1.25 µM eosin Y in DMEM. Viability assays were performed in three biological replicates and are shown as means ± SD. Statistically significant differences in (C), (D), and (E) are indicated: *P < 0.05, **P < 0.01, ***P < 0.001, ****P < 0.0001. N.D., not detectable.